

T-REX: new software for advanced QEXAFS data analysis

Jan Stötzel,^{a*} Dirk Lützenkirchen-Hecht,^a Jan-Dierk Grunwaldt^b and Ronald Frahm^a

^aFachbereich C – Physik, Universität Wuppertal, Gausstrasse 20, D-42097 Wuppertal, Germany, and ^bInstitute for Chemical Technology and Polymer Chemistry, Karlsruhe Institute of Technology, Kaiserstrasse 12, D-76128 Karlsruhe, Germany. E-mail: j.stoetzel@uni-wuppertal.de

New approaches to analyze the data generated by modern time-resolved X-ray absorption spectroscopy instrumentation are presented as part of a new analysis software to handle files containing typically a few thousand EXAFS spectra. Various filter techniques to remove high-frequency noise and run-away values are discussed as well as advanced analysis tools like linear combination fitting, EXAFS fitting, principal component analysis and phase-sensitive detection. These techniques were implemented in a user-friendly graphical user interface to analyse huge data files where it is not possible to treat each spectrum separately. New ideas to exploit existent tools more efficiently for time-resolved EXAFS data analysis are discussed theoretically as well as applied to real measurements, especially *in situ* catalytic experiments and surface-sensitive reflection-mode X-ray absorption studies of thin film growth.

Keywords: QEXAFS; data analysis software; solid-state chemistry; catalysis; grazing-incidence EXAFS.

1. Introduction

The idea of quick-scanning EXAFS (QEXAFS) is to rapidly change the Bragg angle of X-ray monochromator crystals in a continuous and oscillatory manner and thereby to repetitively measure the fine structure at a selected X-ray absorption edge in periods of a few seconds or less (Frahm, 1988, 1989). Nowadays, QEXAFS instrumentation allows the collection of full EXAFS spectra in milliseconds continuously over several hours (Frahm *et al.*, 2005, 2010; Uruga *et al.*, 2007; Khalid *et al.*, 2010; Briois *et al.*, 2011). Invaluable scientific opportunities are the result, as structural and electronic changes during various processes in physics (Frahm *et al.*, 1992; Schroer *et al.*, 2003; Lützenkirchen-Hecht & Frahm, 2006), chemistry (Briois *et al.*, 2005; Okumura *et al.*, 2008; Fujimori *et al.*, 2009; Bauer *et al.*, 2010) and biology (Ascone *et al.*, 2003; Haumann *et al.*, 2005) can be studied. It is thus not surprising that QEXAFS becomes more and more a standard tool in materials science, especially in the context of catalysis research (Clausen *et al.*, 1998; Grunwaldt *et al.*, 2001; Dent, 2002; Bando *et al.*, 2009; Silversmit *et al.*, 2009; Reimann *et al.*, 2011; Föttinger *et al.*, 2011; Rochet *et al.*, 2011). Apart from QEXAFS it is also possible to measure time-resolved EXAFS in energy-dispersive mode by using bent crystals in combination with an array of photodiodes behind the sample (Matsushita & Kaminaga, 1980; Hagelstein *et al.*, 1989; Dent, 2002; Newton *et al.*, 2007), eventually in combination with a slit moving through the

generated polychromatic beam fan in front of the sample (Turbo-XAS) resulting in a sequential QEXAFS-like measurement (Pascarelli *et al.*, 1999).

Although acquisition of many EXAFS spectra each second is nowadays possible by profiting from the high photon flux delivered at third-generation synchrotron sources, the data analysis can be quite time-consuming considering experiments where typically several thousand spectra are generated during only one individual experiment set. Plenty of excellent software is available to analyze up to a few tens of EXAFS spectra such as for example *WinXAS* (Ressler, 1998) or *Athena/Artemis* (Ravel & Newville, 2005) to mention only two. Although most of these programs also provide tools for time-resolved data, they are not designed to work with thousands of spectra. Moreover, the huge number of spectra generated with QEXAFS does not only allow applying standard EXAFS analysis but also more advanced procedures like pattern investigations or the application of special filter techniques and frequency analysis tools. For these reasons we introduce a new software design for the analysis of QEXAFS data measured in absorption, fluorescence or reflection mode using MS Windows systems. The software, named '*Time-resolved EXAFS analysis software*' (in short, *T-REX*), is presented in detail in this paper.

Apart from the description of the various implemented tools, we also present strategies on how to proceed in the course of QEXAFS data analysis and examples from *in situ*

catalysis experiments and surface growth processes. The presented data were all measured at the SuperXAS beamline (Frahm *et al.*, 2010) at the SLS (PSI, Switzerland). It strongly depends on the specific data, whether the herein explained analysis steps are all executable or even required to understand the investigated process. The signal-to-noise ratio has to be considered carefully, before starting for example an EXAFS analysis where good statistics of the order of 10^4 signal-to-noise are prerequisite to obtaining incontestable results. However, in most cases it is only a question of how much time resolution has to be sacrificed to perform a certain analysis. Thus, it is one of the main goals to provide flexible and user-friendly filter tools that allow finding the most suitable compromise between data quality and time resolution.

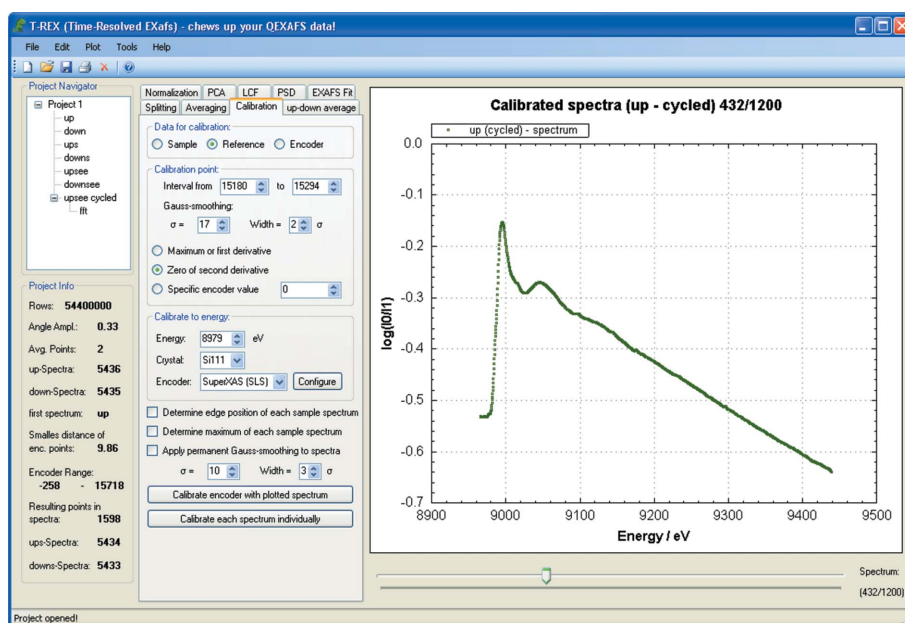


Figure 1 Graphical user interface of *T-REX* showing a spectrum of an oxidized $\text{Cu}/\text{Al}_2\text{O}_3$ catalyst during a modulation cycle with periodically changing oxidizing and reducing applied gas streams.

2. General considerations

The QEXAFS raw data are considered to be written continuously into a single ASCII file consisting of at least two or three columns for the signal of ionization chambers or other detectors and a fourth column for the angular encoder data (Stötzel *et al.*, 2011). ASCII format was chosen here to guarantee compatibility and long time access to QEXAFS data independent of local data processing, which would be an issue with binary input files. Typically 10^3 to 10^6 spectra are scanned in a measurement taking about 10–60 min, which leads to about 10^6 – 10^9 data points. Working with such files in commercial table calculation software is impossible owing to the limits given by the random access memory. Thus, these files have to be processed sequentially and intermediate results have to be stored on hard discs instead of random access memory. With the application of solid state discs this is not a huge disadvantage concerning the performance but programming becomes more sophisticated.

The graphical user interface (GUI) of *T-REX* is shown in Fig. 1. Each QEXAFS file is opened within a new project. Every performed step of QEXAFS data analysis is documented in a navigation tree on the left-hand side of the GUI. Via the entries of this tree the user can navigate to a specific step of the analysis to check the results or to change parameters and repeat the operation. In addition, the project can always be saved, whereby all information required to re-open the project is written to a customized binary file. This is important because the analysis of QEXAFS data can become quite laborious and time-consuming depending on the complexity of the experiment and the amount of data. The tools for data analysis are all located on the tabs adjacent to the navigation tree. A plot pane from the ZedGraph class library (Champion, 2007), which is available under the lesser

Gnu public license (LGPL), is located on the right-hand side of the GUI. After each performed operation, the results are immediately displayed and the graphs can be exported or printed. Below the plot pane a horizontal scroll bar is implemented to allow scrolling through the spectra *via* the mouse or the arrow keys. Thus it is easy to rapidly find and isolate the parts in the data where substantial changes occur.

3. Steps of QEXAFS data analysis

The tools for QEXAFS data analysis are summarized in Fig. 2. They can be arranged in two groups: (i) required initial preparation steps and (ii) various analysis tools. Splitting the data, filtering and energy calibration belong to the first group and have to be applied to all QEXAFS projects. Thereafter, further analysis is possible with the various tools of the second group. Moreover, it has to be distinguished between the tools printed in bold letters in Fig. 2 and the normal printed ones, which are only applicable to experiments where the sample was periodically modulated by a parameter (like temperature, gas composition, gas pressure, *etc.*). Additionally, it is a prerequisite that the induced changes of sample structures are reproducible during the performed modulation cycles. In this case several cycles can be averaged and thereby statistics can be improved without losing time resolution. Furthermore, the application of phase-sensitive detection (PSD), or a reproduction of the dynamics by Fourier series, become feasible, as explained below and in more detail by Stötzel *et al.* (2012a).

3.1. Splitting and sorting raw data

With the application of fast angular encoders in QEXAFS monochromators it became possible to acquire a high-prec-

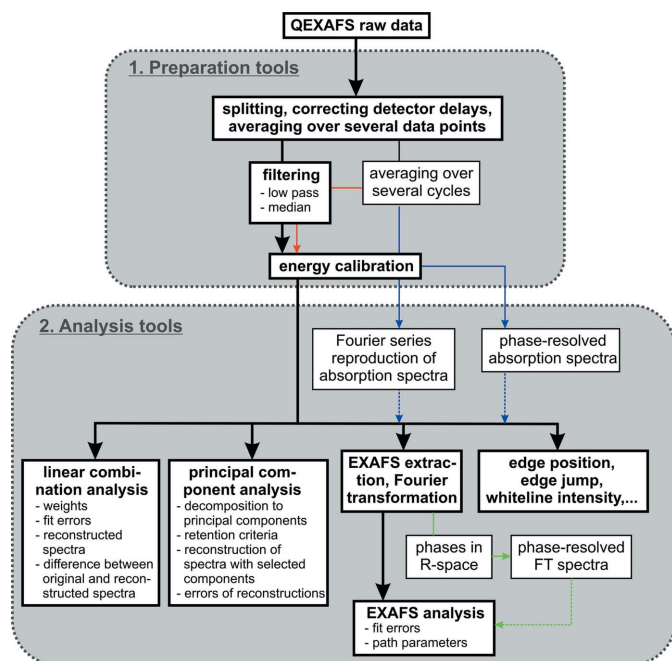


Figure 2
Tools and workflow of QEXAFS data analysis provided in *T-REX*. The tools which are not printed in bold and the coloured arrows indicate steps that depend on modulated experiments as explained in more detail in §3.6. Additionally, analysis tools for reflection-mode EXAFS data evaluation are included.

sion position value synchronized to each absorption value (Stötzel *et al.*, 2008). In the very first step of QEXAFS data analysis this position data is used to split the spectra and to sort them according to the scan direction. Since a time shift between encoder and detector signal has to be considered in fast QEXAFS applications (Stötzel *et al.*, 2011), it is possible to correct this shift during the first step, where the data grid is still very dense and thus good data interpolation is possible. Time shifts can be set individually for each channel to account for different response times of the detectors. Averaging over several raw data points is also possible here if the data density is much higher than required.

A very robust algorithm is required to split the data, especially because scans with varying amplitude and frequency can be performed with new QEXAFS hardware (Stötzel *et al.*, 2010). Experimentally several similar encoder values appear at the reversal points of the oscillatory crystal movement in the case of slow oscillation or high sampling frequencies. Thus, the local symmetry of the curve is exploited in *T-REX* to accurately determine the split position. For this purpose the encoder value is selected, where the added differences of neighbouring encoder value pairs in both directions is lowest. This algorithm can cope with varying frequencies and amplitudes. It turns out to be rather stable even with not perfectly sinusoidal crystal movements.

3.2. Averaging/smoothing spectra

Filtering or averaging is one of the most important steps in QEXAFS data analysis. The time scales of the investigated

processes are usually not known exactly prior to the measurement, so that typically a higher time resolution is chosen than actually required. Subsequent software filtering is the perfect technique to find the most suitable compromise between signal-to-noise ratio and time resolution and thus to optimize the scientific output. Owing to the continuous acquisition of data with constant sampling rates, which are independent of crystal position, interpolation and thus a high data density is required for robust filter processing. Hence, each full EXAFS spectrum should consist of about 2000–5000 points, as these are not evenly distributed over energy owing to the approximately sinusoidal crystal movement using excenter-driven QEXAFS mechanics. There are two different approaches to filtering QEXAFS data: (i) considering each data point as an element, (ii) considering each full spectrum as an element. The first approach is already covered by hardware filters as for example the rise time filter of the current amplifiers. Hereby, the most striking disadvantage is that a constant rise time is used while applying a non-linear scan speed. Also, such a filter is only suitable to filter out very high frequencies, because otherwise the characteristics of the absorption edge and of the XANES features are affected. The second approach allows filtering on time scales similar to those of the investigated process and this approach is exclusively followed here.

Simple averaging by summing up several spectra is the straightforward solution to improve statistics and to reduce the overall number of spectra. Therefore, this approach is often found in the literature. However, depending on the start value where the averaging is started the results are not necessarily unambiguous. This issue is solved by the convolution approach which is described in almost all standard digital signal-processing literature. Mathematically the software filters in *T-REX* for QEXAFS data analysis are a convolution of the X-ray absorption values at each energy position of the spectra $A(E, t)$ as a function of time with a specific kernel $h(t)$,

$$A'(E, t) = \sum_{i=-\infty}^{\infty} A(E, t - t_i) h(t_i). \quad (1)$$

Note that each spectrum is assigned to one time value in this approach. The behaviour of the filter can be tuned *via* the chosen kernel. Various kernels as a function of time are displayed in Fig. 3(a). These correspond (after discretization) to $h(t_i)$ in (1), whereby the kernels have to be chosen in such a way that the sum is finite by introducing a kernel width M . To understand how the filters affect the data, it is useful to display them also in frequency space as done here in Fig. 3(b) for a width M that amounts to 5% of the total number of spectra T . With the spectra-per-second frequency f_m it is possible to analyse dynamics with frequencies up to $0.5f_m$ so that the frequency axis in Fig. 3(b) covers the full dynamic range. The application of a rectangular kernel corresponds to arithmetic averaging and exhibits the strongest low-pass character as shown in Fig. 3(b) (black line). However, high frequencies can still pass the filter (Gibbs phenomenon). Using a rectangular kernel with a width M of five spectra and considering a scan

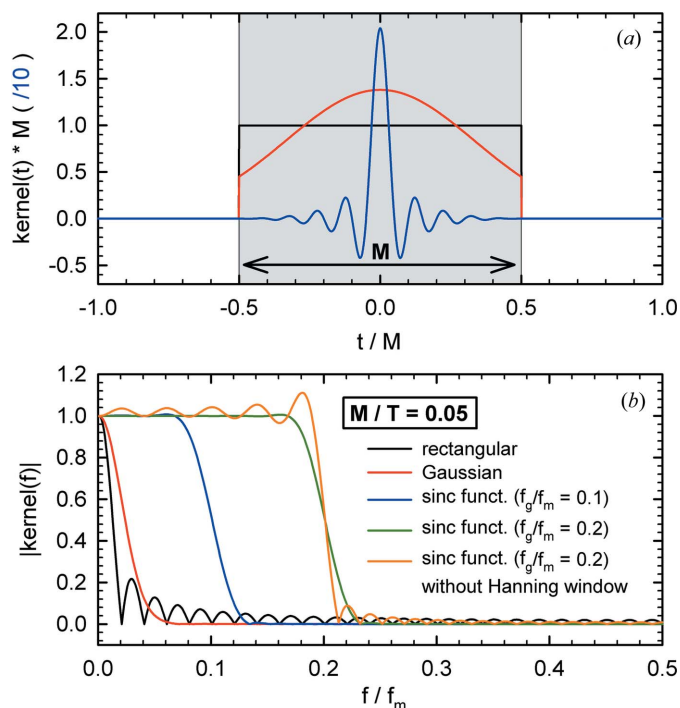


Figure 3

Convolution kernels in (a) time and (b) frequency space that can be used for QEXAFS spectra filtering. Hereby, T is the overall number of spectra in the acquired data file and M is the number of spectra determining the width of the used kernel. The sampling frequency f_m , which is the number of spectra per second here, sets the maximum frequency that can be resolved in the experiment to $0.5f_m$. The sinc function provides an additional parameter f_g , which is used to adjust the cut-off frequency of the low-pass filter.

speed of one spectrum each second, filtering would result in a first spectrum assigned to 2.5 s, which is the result of averaging over the first five spectra. The next one would be the result of averaging over spectra 2–6 and is assigned to the time 3.5 s.

More sophisticated kernels that approach zero at the borders are better suited to suppressing high frequencies entirely. The Gaussian bell function is one convenient solution in this context. Using the same kernel width M as for the rectangular kernel, a weaker low-pass filtering is achieved, but higher frequencies are entirely suppressed [see red line in Fig. 3(b)]. Alternatively, the sinc function can be applied as a more advanced low-pass filter kernel in *T-REX*,

$$h_{\text{sinc}}(t) = \frac{1}{\Sigma_{\text{sinc}}} \frac{1}{2} \underbrace{\left\{ 1 - \cos \left[\frac{2\pi(t - M/2)}{M} \right] \right\}}_{\text{Hanning window}} \underbrace{\frac{\sin(2\pi f_g t)}{2\pi f_g t}}_{\text{sinc function}}. \quad (2)$$

Hereby the normalization factor Σ_{sinc} is the sum over all M kernel values. With the additional parameter f_g the user is able to adjust the cut-off frequency as demonstrated by the blue and green lines in Fig. 3(b). In *T-REX* the sinc function is additionally multiplied with a Hanning window to avoid high-frequency contributions and overshoots. The effect is also demonstrated in Fig. 3(b) (yellow line).

Apart from the pure statistical ‘white’ noise, run-away values might appear in single spectra during QEXAFS

experiments. Sources for these events can be sudden electrical perturbations originating in the data acquisition electronics, a sudden vibration of the sample, a sudden pressure fluctuation inside the ionization chamber (acoustics) or even a beam loss. Moreover, considering liquid samples, bubbles or particles passing the beam path can lead to run-away values and hence distorted spectra. In this context a median filter has proven to be an efficient tool for QEXAFS to sort out single sudden events that are only present in a fraction of data. Thereby access to data is granted which could not be analyzed before [see the example by Reimann *et al.* (2011)]. In this case the high time resolution of modern QEXAFS instrumentation is used to oversample a process, so that several neighbouring spectra can be compared with each other and parts with significant deviations can be discarded without losing much photon statistics.

A combination of median- and low-pass filter can also be applied to the spectra in *T-REX*. Furthermore, it is possible to average the spectra of both scan directions, since two spectra are measured during each monochromator crystal oscillation. To efficiently exploit periodically excited experiments it is also possible to coherently average the spectra acquired during several cycles of the same process, *i.e.* all spectra with the same phase relative to the excitation are summed up. Thus, a fast process can be investigated with significantly better statistics without losing any time resolution. This is a familiar approach considering pump–probe experiments (see, for example, Saes *et al.*, 2004).

3.3. Calibrating spectra

Energy calibration is the final step of the data preparation process in *T-REX* before more sophisticated analysis tools can be applied. With the help of the angular encoder it is sufficient to calibrate all data with one depicted spectrum of the sample or the reference metal foil within *T-REX*. The edge position can either be determined *via* the zero crossing of the second derivative, *via* the maximum of the first derivative, or the edge position is directly linked to a specified encoder value. Thereafter, the edge energy is assigned to the corresponding encoder value and all other values of the spectra are calculated relative to this point. Another smoothing algorithm corresponding to a convolution with a Gaussian bell function is provided here for noisy data. In contrast to the approach presented in the last section, this smoothing is applied only to the selected spectrum along the encoder/energy axis to be able to determine the edge position unambiguously. It is also only applied temporarily for the calibration algorithm. However, with *T-REX* the user can also decide to apply the smoothing permanently for further data analysis, so that kind of a software rise time filter is provided here.

While the calibration step is a prerequisite for further data analysis, two advanced analysis tools can be optionally applied in parallel to the calibration process. First it is possible to exactly determine the edge position of each sample spectrum, which might provide valuable information about changes in the oxidation state (see, for example, Olliges *et al.*, 2012).

Second it is possible to track a specific maximum of the spectra as a function of time, which can be very useful to detect very small changes in the white line feature of transition metals that can be linked to changes in the oxidation state (see, for example, Singh *et al.*, 2010).

3.4. Principal component analysis (PCA)

The PCA is a suitable approach for time-resolved EXAFS analysis, whenever the number of independent species over the course of a reaction is discussed (Fernández-García *et al.*, 1995; Ressler, 1998; Frenkel *et al.*, 2002). As a well established tool, also in other fields like criminology and psychology, the PCA reveals correlations in a set of vectors (EXAFS spectra in the present case) by determining the eigenvalues of the corresponding variance–covariance matrix (see, for example, Dillon & Goldstein, 1984). A crucial issue is the decision criteria to correctly distinguish between independent components and noise contributions. A thorough overview of this topic is given by Hayton *et al.* (2004). Furthermore, the corresponding eigenvectors are mathematical solutions and thus cannot be directly treated as physical species. However, they can be used to reconstruct the spectra with the chosen number of significant eigenvalues. By comparing the reconstructed spectra with the original data there should not appear any significant localized deviation over the course of the reaction, which would indicate a missing component (Wang *et al.*, 2008). Plotting the deviations between original data and reconstructed data as a function of the reaction coordinate is an important approach available in *T-REX* to check whether the considered number of independent species was correct.

Two decision criteria are implemented in *T-REX*. The first one is parallel analysis as introduced by Horn (1965). In this case a second data set with random noise is generated with the same dimensions as the original data set. By additionally applying the PCA to the noise data and thereafter comparing the resulting sorted eigenvalues with those of the original data it is possible to decide which eigenvalues are significant and which can be assigned to random noise. The ‘scree plot’ criterion as a second option (Cattell, 1966; Cattell & Jaspers, 1967) works by linear fitting the tail of eigenvalues that is obviously linked to noise contributions. The first few eigenvalues located above this so-called ‘scree’ are then recognized as significant. Naturally no decision criterion yields correct results in all cases (Hayton *et al.*, 2004). Therefore, both criteria should be applied if possible together with the recombination check described above to reliably determine the number of contributing independent species. An example of

how to use the herein presented PCA tools for *in situ* experiments in catalysis has recently been presented (Stötzel *et al.*, 2012b).

3.5. Linear combination analysis (LCA)

After determining the number of contributing components *via* PCA the next step is their identification. With reference compound spectra the straightforward approach is least-square fits to all normalized spectra over the course of the reaction with a linear combination of the normalized reference spectra. Thereby it can be clarified which reference materials contribute and also to what relative amount (see, for example, Bare *et al.*, 2010; Kleymenov *et al.*, 2012; Langner *et al.*, 2012). In *T-REX* LCA is performed using the *IFEFFIT* code (Newville, 2001) modified to be applicable to several thousand spectra. Details about the application of LCA in X-ray absorption spectroscopy (XAS) can be found for example in the *IFEFFIT* documentation.

To apply LCA in *T-REX* up to five reference spectra can be imported and consistently normalized with the typical XAS background parameters as can be seen in the ‘Components’ box in the LCF tab of the *T-REX* GUI in Fig. 4. Thereafter, the user can choose a range of spectra in the project to be fitted with these references, whereby starting values of weights and energy shifts can be initially guessed or permanently set for each reference individually. Furthermore, the user can choose an energy range in which the fits are performed. Since spectra are scanned in QEXAFS applications and thus different parts of the spectra are measured at different times, it is even possible to repeat the LCA for adjacent energy

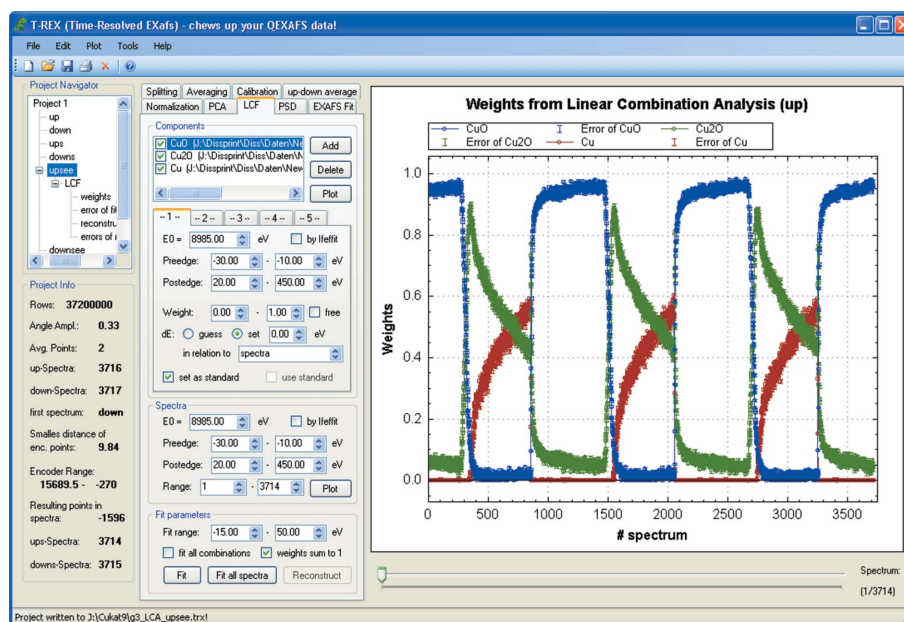


Figure 4

Linear combination analysis of XANES spectra at the Cu *K*-edge of a Cu/Al₂O₃ catalyst during an applied gas flow alternating each 60 s between 21%–O₂/He and 5%–H₂/He. The normalized 3714 sample spectra were least-square fitted by a linear combination of normalized reference spectra of Cu (red), Cu₂O (green) and CuO (blue). Fractions of each Cu species are plotted in *T-REX* as a function of spectrum number, whereby ten spectra correspond to 1 s acquisition time in this example. The reproducible sample variation between more reduced and more oxidized copper species can be easily followed here.

intervals and thereby to further increase the time resolution beyond the one determined by the crystal oscillation frequency.

As also visible in the GUI in Fig. 4, LCA can be performed for one single spectrum or for a chosen interval of spectra. Additionally, it is possible to set up the fit so that all possible combinations of references are fitted to the spectra of the experiment, which can be very helpful if the sample composition drastically changes during an experiment and some components suddenly vanish or appear. It was recognized as an essential feature that during the LCA fitting process the user can follow the evolution of calculated weights on the plot pane and also abort the operation as soon as weird results appear. This is because the LCA operation for a few thousand spectra can take a few hours. After the operation it is also possible to plot the reconstructed spectra or the fit errors as a function of the reaction coordinate. These results are accessible *via* the ‘Project Navigator’ on the left-hand side of the *T-REX* GUI. Performing the LCA for several thousand spectra is possible as also demonstrated in Fig. 4, where the oxidation/reduction behaviour of $\text{Cu}/\text{Al}_2\text{O}_3$ was studied by fitting the measured data with Cu , Cu_2O and CuO reference spectra. In this experiment the gas stream applied to the catalyst was switched between 5% H_2/He and 21% O_2/He every 60 s, while QEXAFS spectra were acquired with a crystal oscillation frequency of 10 Hz resulting in 20 full EXAFS spectra each second [see Stötzel *et al.* (2009) for experimental details]. This example demonstrates how valuable the LCA approach for studying fast processes by resolving the sample composition is. The information of thousands of spectra is summarized in a plot, which is easy to obtain and easy to understand.

3.6. Exploiting modulated excitation experiments

The periodic excitation of a process leading to reproducible structural changes of the sample can be exploited to improve statistics by averaging over several cycles, which is a straightforward step in *T-REX*. Furthermore, it is possible to reproduce the data of the resulting averaged cycle with the basic frequency of the modulation and higher harmonics only. This approach is based on the assumption that all other frequencies can be assigned to noise contributions. Technically, this reproduction is achieved by calculating the Fourier coefficients of the absorption data as a function of time at each energy value of the spectra and thereafter building the Fourier sums

$$\begin{aligned}
 A(E, t) &= A_0(E) + \sum_{n=1}^{\infty} [A_n(E) \cos(n\omega t) + B_n(E) \sin(n\omega t)], \\
 A_0(E) &= (1/T) \int_0^T A(E, t) dt, \\
 A_n(E) &= (2/T) \int_0^T A(E, t) \cos(n\omega t) dt, \\
 B_n(E) &= (2/T) \int_0^T A(E, t) \sin(n\omega t) dt, \quad (3)
 \end{aligned}$$

with $\omega = 2\pi/T$ and period T . Thereby, it is possible to adjust the number of contributing orders *via* an upper limit for n . Confining n to low values is equivalent to cutting off high frequencies and is therefore a kind of low-pass filter, which often helps to substantially improve data quality. However, since the coefficients are calculated for each energy value separately, some correlations in energy usually are lost. This is a significant drawback compared with the filter approach presented in §3.2, where the whole spectrum is considered as one unit. Accordingly, further EXAFS data analysis of the reproduced spectra has to be performed carefully which is the reason for the coloured thin arrows that appear in Fig. 2 in the context of such operations.

With the Fourier coefficients it is also possible to perform phase-sensitive detection (PSD) according to (Baurecht & Fringeli, 2001)

$$\begin{aligned}
 A_n^{\text{PSD}}(E) &= (2/T) \int_0^T A(E, t) \sin(n\omega t + \varphi_n^{\text{PSD}}) dt \\
 &= B_n \cos(\varphi_n^{\text{PSD}}) + A_n \sin(\varphi_n^{\text{PSD}}), \quad (4)
 \end{aligned}$$

which is, for example, applied in IR spectroscopy, X-ray diffraction and Raman spectroscopy (see, for example, Urakawa *et al.*, 2008, 2011). Applied to QEXAFS it is possible to compare the computed first-order PSD spectra for various phases with difference spectra of reference materials and thereby to identify intermediate states and increase surface sensitivity (Ferri *et al.*, 2010, 2011).

The Fourier coefficients can also be used to calculate the phases for each order and at each energy value directly with

$$\varphi_n(E) = \tan^{-1}[A_n(E)/B_n(E)]. \quad (5)$$

Now, if different parts of the spectrum are reproduced with different phases of, for example, the first-order contribution, this leads to new insights in the dynamics and can help to identify intermediate states. The major drawback of applying equations (3) or (4) to absorption spectra is that the contribution of each species is distributed over the full EXAFS range and not localized at a specific energy as for the other spectroscopic techniques mentioned above. Thus, in *T-REX* it is not only possible to calculate the Fourier coefficients of the absorption data but also of the Fourier-transformed EXAFS, which yields a pseudo radial distribution function of neighbour atoms. Here, it is indeed possible to assign different phases to different local environments and thereby to better understand the investigated reaction.

All the tools for modulated experiments are presented in more detail in a forthcoming publication, where they are also compared with the straightforward approach of filtering the data with the tools presented in §3.2 followed by conventional EXAFS analysis (Stötzel *et al.*, 2012a). The calculation of $A_0(E)$ [see equation (3)] can also be helpful in non-modulated experiments, as it is the mean spectrum of the entire data set. Subtracting it from all spectra leads to difference EXAFS spectra with which it is easier to detect systematic changes during an investigated process (Ramaker & Koningsberger, 2010).

3.7. Background subtraction, spline fitting, Fourier transformation

One crucial aim of *T-REX* is to exploit the full potential of QEXAFS measurements that consist of several thousand full EXAFS spectra, each including information on the local structure around the edge element. Parameters are the type of neighbouring atoms, coordination numbers, bond lengths

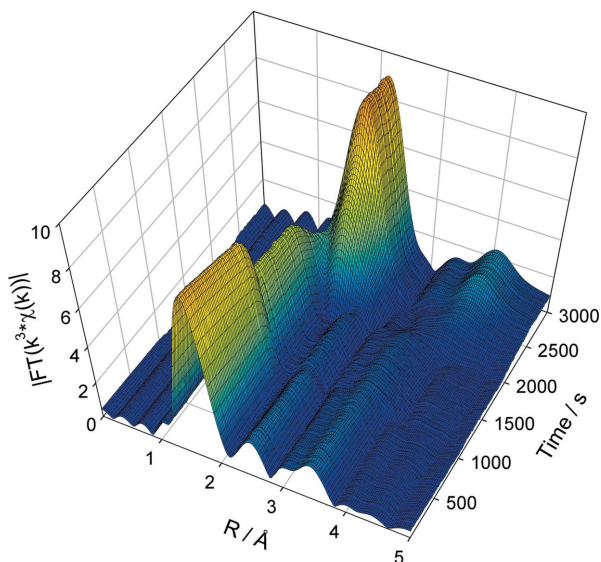
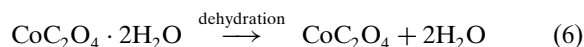
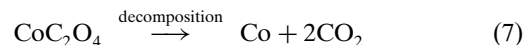


Figure 5 Fourier-transformed k^3 -weighted EXAFS spectra at the Co K -edge measured during the thermal decomposition of Co oxalate in H_2 gas flow (k -range: 2.4 – 9.15 \AA^{-1}). The temperature was increased linearly from room temperature to 673 K and the two stages of oxalate dehydration (two of six oxygen neighbours removed) and of oxalate decomposition (evolution of Co metal as final product) can be identified immediately in the data.

and lattice disorders. For that purpose the *IFEFFIT* tools (Newville, 2001) for normalizing spectra, extracting the EXAFS $\chi(k)$ and calculating the Fourier transformations are implemented in such a way that they can be applied to a single spectrum as well as to all spectra of the project. The results are written into multi-column files that are used for further analysis as PCA and EXAFS fitting or can be used directly for a more qualitative data analysis. As an example the Fourier-transformed EXAFS data during thermal decomposition of Co oxalate in H_2 (e.g. Dollimore, 1987; Maciejewski *et al.*, 2000; Lützenkirchen-Hecht *et al.*, 2005a) are shown in Fig. 5. The oxalate was filled into a cell designed for X-ray absorption experiments in heterogeneous catalysis (Grunwaldt *et al.*, 2004) and measurements were performed at the Co K -edge with a scan range from 7700 eV to 8044 eV , leading to an upper limit for the photoelectron wavenumber of $k = 9.15 \text{ \AA}^{-1}$ for the Fourier transformation. Without further analysis the user can immediately detect the dehydration



starting at about 1000 s (at $\sim 433 \text{ K}$). Here the contribution of the first oxygen shell decreases by approximately 33% , caused by the release of water and thus removal of two of the six oxygen neighbours. Furthermore, also the slight decrease in the Co–O bond distance from about 2.08 \AA to 2.03 \AA is obvious, as detailed in Fig. 6. After about 1800 s at $\sim 548 \text{ K}$ the decomposition starts with the evolution of metallic Co according to



as recognizable by the typical shell distribution for f.c.c./h.c.p. lattice types at the end of the reaction.

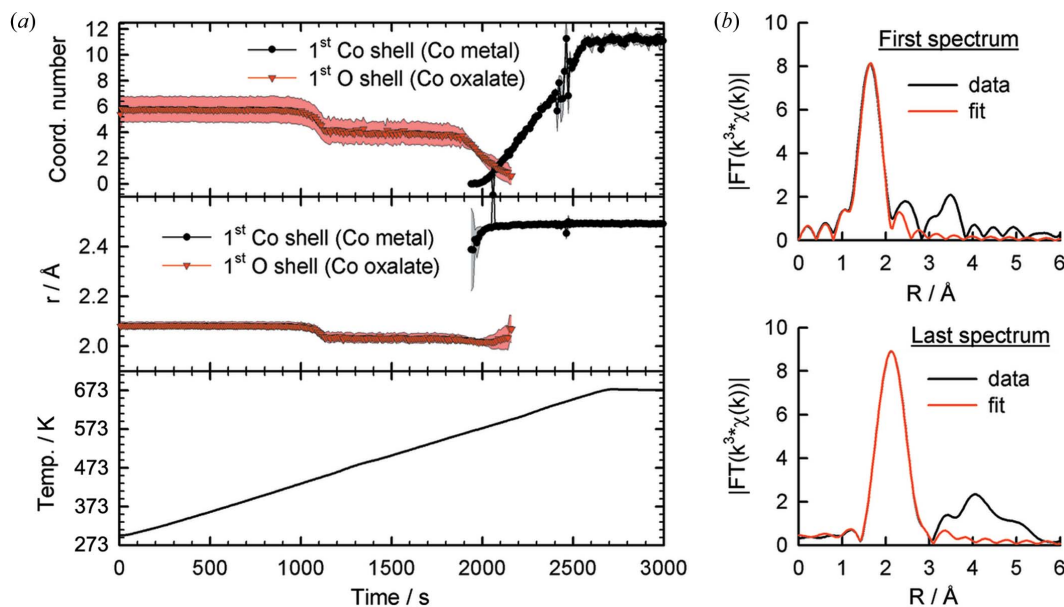


Figure 6 (a) First-shell EXAFS data fitting during the thermal decomposition of Co oxalate with the first Co–O scattering path of Co oxalate and at the end of the experiment the first Co–Co path of the formed metallic cobalt. Coordination numbers and atomic distance values are plotted as a function of reaction time as well as the applied temperature ramp. The removal of two oxygen neighbours and the decrease of the distance between the remaining oxygen neighbours and the central Co atom is clearly recognizable at about 1100 s (453 K) owing to dehydration. The Co metal at the end of the reaction evolves linearly, and pure Co is obtained before the final temperature is reached. (b) Exemplary EXAFS fits from which the results in (a) were derived.

3.8. EXAFS fitting

With the extracted part of the EXAFS data $\chi(k)$ it is possible to directly perform EXAFS fits in *T-REX*. Prerequisite is the input file 'feff.inp' that contains an initially suggested structure model. This file can be directly imported and the corresponding scattering paths are calculated using the *FEFF6* code (Zabinsky *et al.*, 1995). Next *FEFFIT* (Newville *et al.*, 1995) is used to perform EXAFS fits by refining the parameters of selected paths, which are the amplitude factor NS_0^2 , the energy shift ΔE , the path length deviation ΔR and the mean square displacement σ^2 . Fitting EXAFS with *T-REX* is straightforward to perform, especially for those who are familiar with *Artemis* (Ravel & Newville, 2005). It is also possible to set path parameters to a constant value or to let them be determined by the fit, while the fit range and the k -weighting can be varied. However, the software is designed in such a way that the fits are performed for thousands of spectra and the results of all fits are written into one file. Thus, it is easily possible to plot parameters as the coordination number of a selected shell or its distance to the absorbing atom as a function of the reaction coordinate. Exemplarily this is shown in Fig. 6(a) for the first oxygen shell of Co oxalate and the first Co shell of Co metal during thermal decomposition in H_2 as discussed above. Exemplary EXAFS fits for the start and the end of the reaction are shown in Fig. 6(b). As already explained for the LCF, it is again possible to follow the results already during the fit operation and to abort the operation in case of, for example, obviously poorly chosen parameters that lead to unreasonable results.

3.9. Simulation tool for grazing-incidence EXAFS in reflection mode

Various experiments have proven that using QEXAFS in grazing-incidence mode close to the total reflection is a promising approach to gain new insights in the *in situ* deposition of and reactions on thin films with second time resolution (Frahm *et al.*, 1991; Lützenkirchen-Hecht & Frahm, 2005b, 2006) and recently also sub-second time resolution as demonstrated here. Owing to the close relationship between reflection and absorption data by means of the Kramers–Kronig relation, the full EXAFS information is also included in the reflectivity spectra. However, in the atomic structure, changes in film thickness and roughness can also be determined. Using the distorted-wave Born approximation theory the spectra can be simulated by including the specific geometrical parameters of the performed experiment, such as for example beam dimensions, incident and exit angle, size of entrance and exit slit system and the sample–detector distance (Holý *et al.*, 1993, 1999; Holý & Baumbach, 1994). By varying the layer and substrate parameters (density, thickness, roughness and correlation length) the simulation can be modified until the results are congruent with the measured spectra. For this purpose a corresponding simulation tool is included in *T-REX*, as displayed in Fig. 7(a). Several spectra can be imported and several simulations can be performed in one project. Prerequisite for the simulations is a file containing

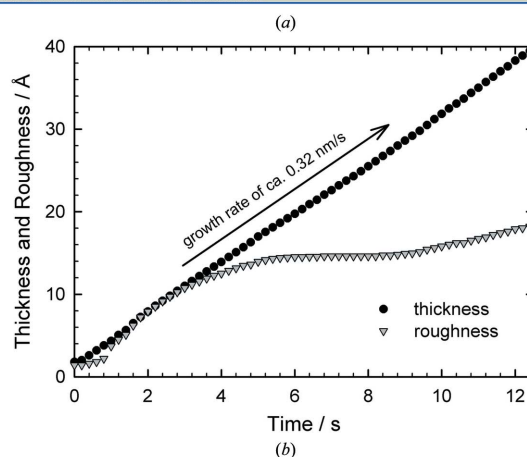
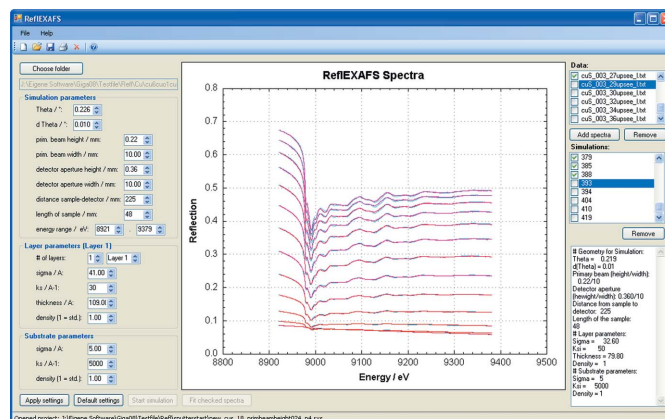


Figure 7

QEXAFS analysis of data taken in the reflection mode during *in situ* DC magnetron sputtering of a Cu layer on a glass substrate. Sputtering was performed in pure Ar at room temperature and the spectra were measured using an incident angle of 0.25° . (a) Simulation tool in *T-REX* for calculating reflection spectra before comparing them with the measured data. Measured spectra are displayed in red, the simulated ones in blue. By refining the calculations it is then possible to extract the layer composition, thickness and roughness as well as the substrate roughness in the case of very thin layers. (b) Extracted thickness and roughness of the Cu layer as a function of sputter time using the simulation tool.

the optical data of substrate and layer material, namely the dispersion $\delta(E)$ and the absorption term $\beta(E)$ in the energy range of the spectra. Since it can be a time-consuming task to simulate tens or hundreds of spectra, it is possible to save the current work with all loaded spectra, performed simulations and all settings as a separate binary file, which can be distributed and re-opened again.

An example for results obtained with this simulation tool is displayed in Fig. 7(b). Here, pure Cu was deposited on a glass substrate at room temperature by DC magnetron sputtering, while *in situ* QEXAFS measurements were performed in reflection mode using incident and exit angles of 0.25° , which are below the critical angle of total reflection of metallic Cu. The layer thickness and roughness parameters for the best fits are shown for the first 12.5 s with a time resolution of 200 ms. Detailed insights into the layer growth process are achievable, as it is for example possible to determine the constant growth rate of about 0.32 nm s^{-1} , as expected from the sputtering conditions with constant Ar gas pressure, discharge voltage

and current. In contrast, while the roughness also follows an almost linear increase for the first 3 s, it appears to be constant between 6 and 8 s of sputtering. Moreover, the fits have shown that the optical data of pure Cu are not appropriate to fit the measured data satisfactorily in both XANES and EXAFS regions. Instead, a mixture of 60% Cu, 30% Cu₂O and 10% CuO yields the best results for the initial layer growth which is most likely due to residual water/oxygen molecules on the substrate. Thus, it is possible to resolve the atomic structure and the layer morphology during layer growth processes with sub-second time resolution when using QEXAFS in reflection mode and analysing the data with *T-REX*. More details and examples for surface-sensitive QEXAFS measurements will be the topic of forthcoming publications.

4. Conclusions

A new data analysis software for efficient QEXAFS data analysis has been developed, which is capable of performing the typical steps of EXAFS and XANES data analysis but now for several thousand spectra. Moreover, a substantial set of digital filter tools is provided to deal with white noise as well as run-away values in a flexible way. This especially allows realistic heterogeneous systems to be studied in solid state chemistry and catalysis. Strategies towards how to better exploit the information in time-resolved EXAFS experiments were presented, considering also modulated experiments. A simulation tool to deal with data measured in reflection mode at grazing incidence was added for the investigation of layer morphologies during *in situ* layer deposition or layer corrosion processes. Thus, the presented software *T-REX* will be a valuable help for users with the cumbersome processing of thousands of EXAFS spectra, which is also important considering technical advances in the future to further increase the time resolution for EXAFS applications.

T-REX can be obtained by directly contacting the authors. A website with documentation and download link is under construction.

We acknowledge the Swiss Light Source for beam time and M. Nachttegaal for support at the SuperXAS beamline.

References

Ascone, I., Meyer-Klaucke, W. & Murphy, L. (2003). *J. Synchrotron Rad.* **10**, 16–22.

Bando, K. K., Wada, T., Miyamoto, T., Miyazaki, K., Takakusagi, S., Gott, T., Yamaguchi, A., Nomura, M., Oyama, S. T. & Asakura, K. (2009). *J. Phys. Conf. Ser.* **190**, 012158.

Bare, S. R., Kelly, S. D., Ravel, B., Greenlay, N., King, L. & Mickelson, G. E. (2010). *Phys. Chem. Chem. Phys.* **12**, 7702–7711.

Bauer, M., Heusel, G., Mangold, S. & Bertagnolli, H. (2010). *J. Synchrotron Rad.* **17**, 273–279.

Baurecht, D. & Fringeli, U. P. (2001). *Rev. Sci. Instrum.* **72**, 3782.

Briois, V., Fonda, E., Belin, S., Barthe, L., La Fontaine, C., Langlois, F., Ribbens, M. & Villain, F. (2011). *UVX 2010 – 10e Colloque sur les Sources Cohérentes et Incohérentes UV, VUV et X; Applications et Développements Récents*, pp. 41–47. EDP Sciences.

Briois, V., Lützenkirchen-Hecht, D., Villain, F., Fonda, E., Belin, S., Griesebock, B. & Frahm, R. (2005). *J. Phys. Chem. A*, **109**, 320–329.

Cattell, R. B. (1966). *Multivar. Behav. Res.* **1**, 245–276.

Cattell, R. B. & Jaspers, J. (1967). *Multivar. Behav. Res. Monographs* **3**, 1–212.

Champion, J. (2007). *A flexible charting library for. NET*, <http://www.codeproject.com/Articles/5431/A-flexible-charting-library-for-.NET>.

Clausen, B. S., Topsøe, H. & Frahm, R. (1998). *Adv. Catal.* **42**, 315–344.

Dent, A. J. (2002). *Top. Catal.* **18**, 27–35.

Dillon, W. R. & Goldstein, M. (1984). *Multivariate Analysis*. New York: Wiley.

Dollimore, D. (1987). *Thermochim. Acta*, **117**, 331–363.

Fernández-García, M., Márquez Alvarez, C. & Haller, G. L. (1995). *J. Phys. Chem.* **99**, 12565–12569.

Ferri, D., Kumar, M. S., Wirz, R., Eyssler, A., Korsak, O., Hug, P., Weidenkaff, A. & Newton, M. A. (2010). *Phys. Chem. Chem. Phys.* **12**, 5634–5646.

Ferri, D., Newton, M. A. & Nachttegaal, M. (2011). *Top. Catal.* **54**, 1070–1078.

Föttinger, K., van Bokhoven, J. A., Nachttegaal, M. & Rupprechter, G. (2011). *J. Phys. Chem. Lett.* **2**, 428–433.

Frahm, R. (1988). *Nucl. Instrum. Methods Phys. Res. A*, **270**, 578–581.

Frahm, R. (1989). *Rev. Sci. Instrum.* **60**, 2515–2518.

Frahm, R., Barbee, T. W. Jr & Warburton, W. (1991). *Phys. Rev. B*, **44**, 2822–2825.

Frahm, R., Nachttegaal, M., Stötzel, J., Harfouche, M., van Bokhoven, J. A. & Grunwaldt, J.-D. (2010). *AIP Conf. Proc.* **1234**, 251–255.

Frahm, R., Richwin, M. & Lützenkirchen-Hecht, D. (2005). *Phys. Scr.* **T115**, 974–976.

Frahm, R., Wong, J., Holt, J. B., Larson, E. M., Rupp, B. & Waide, P. A. (1992). *Phys. Rev. B*, **46**, 9205–9208.

Frenkel, A. I., Kleifeld, O., Wasserman, S. R. & Sagi, I. (2002). *J. Chem. Phys.* **116**, 9449–9456.

Fujimori, T., Takaoka, M., Tanino, Y., Oshita, K. & Morisawa, S. (2009). *J. Phys. Conf. Ser.* **190**, 012183.

Grunwaldt, J.-D., Basini, L. & Clausen, B. S. (2001). *J. Catal.* **200**, 321–329.

Grunwaldt, J.-D., Caravati, M., Hannemann, S. & Baiker, A. (2004). *Phys. Chem. Chem. Phys.* **6**, 3037–3047.

Hagelstein, M., Cunis, S., Frahm, R., Niemann, W. & Rabe, P. (1989). *Physica B*, **158**, 324–325.

Haumann, M., Liebisch, P., Müller, C., Barra, M., Grabolle, M. & Dau, H. (2005). *Science*, **310**, 1019–1021.

Hayton, J. C., Allen, D. G. & Scarpello, V. (2004). *Organ. Res. Methods*, **7**, 191–205.

Holý, V. & Baumbach, T. (1994). *Phys. Rev. B*, **49**, 10668–10676.

Holý, V., Kubéna, J., Ohlidal, I., Lischka, K. & Plotz, W. (1993). *Phys. Rev. B*, **47**, 15896–15903.

Holý, V., Pietsch, U. & Baumbach, T. (1999). *High Resolution X-ray Scattering from Thin Films and Multilayers, Springer Tracts in Modern Physics*, Vol. 149, pp. 1–251.

Horn, J. L. (1965). *Psychometrika*, **32**, 179–185.

Khalid, S., Caliebe, W., Siddons, P., So, I., Clay, B., Lenhard, T., Hanson, J., Wang, Q., Frenkel, A. I., Marinkovic, N., Hould, N., Ginder-Vogel, M., Landrot, G. L., Sparks, D. L. & Ganjoo, A. (2010). *Rev. Sci. Instrum.* **81**, 015105.

Kleymenov, E., Sa, J., Abu-Dahrieh, J., Rooney, D., van Bokhoven, J. A., Troussard, E., Szlachetko, J., Safonova, O. & Nachttegaal, M. (2012). *Catal. Sci. Technol.* doi:10.1039/c1cy00277e.

Langner, P., Mikutta, C. & Kretzschmar, R. (2012). *Nat. Geosci.* **5**, 66–73.

Lützenkirchen-Hecht, D. & Frahm, R. (2005b). *Thin Solid Films*, **493**, 67–76.

Lützenkirchen-Hecht, D. & Frahm, R. (2006). *Surf. Sci.* **600**, 4380–4384.

Lützenkirchen-Hecht, D., Grunwaldt, J.-D., Richwin, M., Griesebock, B., Baiker, A. & Frahm, R. (2005a). *Phys. Scr.* **T115**, 831.

Maciejewski, M., Ingier-Stocka, E., Emmerich, W.-D. & Baiker, A. (2000). *J. Therm. Anal. Calorim.* **60**, 735–758.

- Matsushita, T. & Kaminaga, U. (1980). *J. Appl. Cryst.* **13**, 465–471.
- Newton, M. A., Dent, A. J., Fiddy, S. G., Jyoti, B. & Evans, J. (2007). *Catal. Today*, **126**, 64–72.
- Newville, M. (2001). *J. Synchrotron Rad.* **8**, 322–324.
- Newville, M., Ravel, B., Haskel, D., Rehr, J. J., Stern, E. A. & Yacoby, Y. (1995). *Physica B*, **208–209**, 154–156.
- Okumura, K., Honma, T., Hirayama, S., Sanada, T. & Niwa, M. (2008). *J. Phys. Chem. C*, **112**, 16740–16747.
- Olliges, I., Stötzel, J., Koziej, D., Rossell, M. D., Grunwaldt, J.-D., Nachttegaal, M., Frahm, R. & Niederberger, M. (2012). *Chem. Eur. J.* **18**, 2305–2312.
- Pascarelli, S., Neisius, T. & De Panfilis, S. (1999). *J. Synchrotron Rad.* **6**, 1044–1050.
- Ramaker, D. E. & Koningsberger, D. C. (2010). *Phys. Chem. Chem. Phys.* **12**, 5514–5534.
- Ravel, B. & Newville, M. (2005). *J. Synchrotron Rad.* **12**, 537–541.
- Reimann, S., Stötzel, J., Frahm, R., Kleist, W., Grunwaldt, J. D. & Baiker, A. (2011). *J. Am. Chem. Soc.* **133**, 3921–3930.
- Ressler, T. (1998). *J. Synchrotron Rad.* **5**, 118–122.
- Rochet, A., Moizan, V., Pichon, C., Diehl, F., Berliet, A. & Briois, V. (2011). *Catal. Today*, **171**, 186–191.
- Saes, M., van Mourik, F., Gawelda, W., Kaiser, M., Chergui, M., Bressler, C., Grolimund, D., Abela, R., Glover, T. E., Heimann, P. A., Schoenlein, R. W., Johnson, S. L., Lindenberg, A. M. & Falcone, R. W. (2004). *Rev. Sci. Instrum.* **75**, 24.
- Schroer, C. G., Kuhlmann, M., Günzler, T. F., Lengeler, B., Richwin, M., Griesebock, B., Lützenkirchen-Hecht, D., Frahm, R., Ziegler, E., Mashayekhi, A., Haeffner, D. R., Grunwaldt, J.-D. & Baiker, A. (2003). *Appl. Phys. Lett.* **82**, 3360–3362.
- Silversmit, G., Poelman, H., Balcaen, V., Heynderickx, P. M., Olea, M., Nikitenko, S., Bras, W., Smet, P. F., Poelman, D., de Gryse, R., Reniers, M.-F. & Marin, G. B. (2009). *J. Phys. Chem. Solids*, **70**, 1274–1284.
- Singh, J., Nachttegaal, M., Alayon, E. M. C., Stötzel, J. & van Bokhoven, J. A. (2010). *ChemCatChem*, **2**, 653–657.
- Stötzel, J., Frahm, R., Kimmerle, B., Nachttegaal, M. & Grunwaldt, J.-D. (2012b). *J. Phys. Chem. C*, **116**, 599–609.
- Stötzel, J., Lützenkirchen-Hecht, D., Fonda, E., De Oliveira, N., Briois, V. & Frahm, R. (2008). *Rev. Sci. Instrum.* **79**, 083107.
- Stötzel, J., Lützenkirchen-Hecht, D. & Frahm, R. (2010). *Rev. Sci. Instrum.* **81**, 073109.
- Stötzel, J., Lützenkirchen-Hecht, D. & Frahm, R. (2011). *J. Synchrotron Rad.* **18**, 165–175.
- Stötzel, J., Lützenkirchen-Hecht, D., Frahm, R. & Grunwaldt, J.-D. (2012a). In preparation.
- Stötzel, J., Lützenkirchen-Hecht, D., Frahm, R., Kimmerle, B., Baiker, A., Nachttegaal, M., Beier, M. J. & Grunwaldt, J.-D. (2009). *J. Phys. Conf. Ser.* **190**, 012153.
- Urakawa, A., Bürgi, T. & Baiker, A. (2008). *Chem. Eng. Sci.* **63**, 4902–4909.
- Urakawa, A., van Beek, W., Monrabal-Capilla, M., Galán-Mascarós, J. R., Palin, L. & Milanese, M. (2011). *J. Phys. Chem. C*, **115**, 1323–1329.
- Uruga, T., Tanida, H., Inoue, K., Kamazaki, H. & Irie, T. (2007). *AIP Conf. Proc.* **882**, 914–916.
- Wang, Q., Hanson, J. C. & Frenkel, A. I. (2008). *J. Chem. Phys.* **129**, 234502.
- Zabinsky, S. I., Rehr, J. J., Ankudinov, A., Albers, R. C. & Eller, M. J. (1995). *Phys. Rev. B*, **52**, 2995–3009.